





Structural and mechanistic insights into the precise product synthesis by a *bifunctional* miltiradiene synthase

Yuru Tong^{1,2,†} , Xiaoli Ma^{3,†} , Tianyuan Hu², Kang Chen¹, Guanghong Cui¹, Ping Su¹, Haifeng Xu^{3,4}, Wei Gao^{5,*} , Tao Jiang^{3,4,*}  and Luqi Huang^{1,*}

¹National Resource Center for Chinese Materia Medica, China Academy of Chinese Medical Sciences, Beijing, China

²School of Pharmaceutical Sciences, Capital Medical University, Beijing, China

³National Laboratory of Biomacromolecules, Institute of Biophysics, Chinese Academy of Sciences, Beijing, China

⁴University of Chinese Academy of Sciences, Beijing, China

⁵Beijing Shijitan Hospital, Capital Medical University, Beijing, China

Received 15 January 2022;

revised 22 July 2022;

accepted 14 September 2022.

*Correspondence (Tel +86-010-64888508;

fax +86-010-64889252; email

tjiang@ibp.ac.cn (TJ); Tel +86-10-83916572;

fax +86-010-83916572; email

weigao@ccmu.edu.cn (WG); Tel +86-010-

64014411; fax +86-010-64013996; email

huangluqi01@126.com (LH)

[†]Passed away on May 11, 2022.

[‡]These authors contributed equally to this work.

Summary

Selaginella moellendorffii miltiradiene synthase (*SmMDS*) is a unique bifunctional diterpene synthase (diTPS) that catalyses the successive cyclization of (*E,E,E*)-geranylgeranyl diphosphate (GGPP) via (+)-copalyl diphosphate (CPP) to miltiradiene, which is a crucial precursor of important medicinal compounds, such as triptolide, ecabet sodium and carnosol. Miltiradiene synthetic processes have been studied in monofunctional diTPSs, while the precise mechanism by which active site amino acids determine product simplicity and the experimental evidence for reaction intermediates remain elusive. In addition, how bifunctional diTPSs work compared to monofunctional enzymes is attractive for detailed research. Here, by mutagenesis studies of *SmMDS*, we confirmed that pimar-15-en-8-yl⁺ is an intermediate in miltiradiene synthesis. Moreover, we determined the apo-state and the GGPP-bound state crystal structures of *SmMDS*. By structure analysis and mutagenesis experiments, possible contributions of key residues both in class I and II active sites were suggested. Based on the structural and functional analyses, we confirmed the copal-15-yl⁺ intermediate and unveiled more details of the catalysis process in the *SmMDS* class I active site. Moreover, the structural and experimental results suggest an internal channel for (+)-CPP produced in the class II active site moving towards the class I active site. Our research is a good example for intermediate identification of diTPSs and provides new insights into the product specificity determinants and intermediate transport, which should greatly facilitate the precise controlled synthesis of various diterpenes.

Keywords: miltiradiene, copalyl diphosphate, crystal structure, mechanism, channel.

Introduction

Diterpenes constitute a large family of natural products. According to backbone structure, diterpenes can be categorized as abietanes, pimaranes, kaurenes, labdanes and fusicocanones (Hanson *et al.*, 2019). Diterpenes are diverse in structure and stereochemistry, especially abietane-type diterpenes, thereby providing abundant sources for drug discovery. Triptolide and its analogues exhibit anticancer activity in multiple cancers, including pancreatic cancer (Ding *et al.*, 2017), breast cancer (He *et al.*, 2020) and glioma (Liu *et al.*, 2019). The anti-ulcer agent ecabet sodium is a dehydroabietic acid derivative prepared from pine resin. Carnosol, an abietane-type diterpene, exhibits anti-inflammatory and anticancer activities (Johnson, 2011; Shi *et al.*, 2020; Figure 1a). Due to its high medical value, different approaches to synthesize abietane-type diterpenes have been explored. When focusing on the chemical synthesis or the enzymatic reaction of therapeutic natural products, we face an interesting question regarding the mechanisms by which the synthetic process selects a particular isomer of a complex molecule (Hong and Tantillo, 2014). Considering that the cyclization reactions catalysed by diterpene synthases (diTPSs) show high substrate selectivity and product stereospecificity, diTPSs have become a good target system for structural and functional studies to answer this question.

The diversity of diterpenes derived from the (*E,E,E*)-geranylgeranyl diphosphate (GGPP) precursor is determined by stereochemically controlled class II and class I diTPS combinations (Andersen-Ranberg *et al.*, 2016; Christianson, 2017). The enzymatic synthesis of miltiradiene, the key backbone precursor of abietane-type diterpenes, has attracted considerable attentions. Usually, miltiradiene is synthesized through a two-step cyclization reaction that includes sequential conversion of GGPP via (+)-copalyl diphosphate (CPP) to miltiradiene (Gao *et al.*, 2009). Recently, monofunctional class II diTPS and class I diTPS for biosynthetic miltiradiene have been isolated from seven angiosperm plants (Bozic *et al.*, 2015; Bruckner *et al.*, 2014; Cui *et al.*, 2015; Gao *et al.*, 2009; Jin and Cui, 2017; Pateraki *et al.*, 2014; Su *et al.*, 2018; Zerbe *et al.*, 2014). In one case, however, a bifunctional diTPS with two independent active sites (class II/class I) was discovered in *Selaginella moellendorffii* (*S. moellendorffii* miltiradiene synthase, *SmMDS*; Sugai *et al.*, 2011). Previously, we applied modular pathway and chimeric diTPS engineering attempts for the high production of miltiradiene in yeast (Hu *et al.*, 2020; Zhou *et al.*, 2012b). However, few reports on the structural mechanism of diTPSs can provide structural basis for directed enzyme evolution.

To date, the crystal structure of only three plant diTPSs has been reported, namely monofunctional taxadiene synthase from *Taxus brevifolia* (*TbTS*; Koksall *et al.*, 2011), monofunctional *ent-*

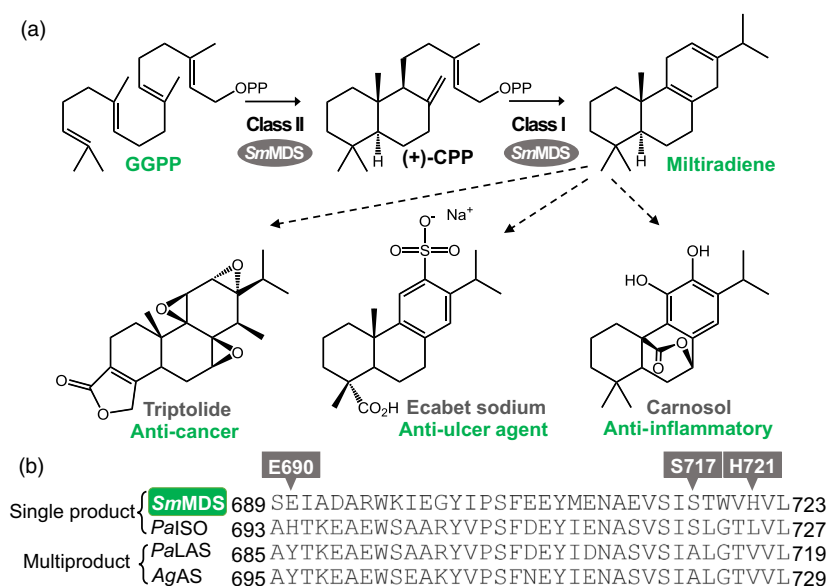


Figure 1 The biosynthesis pathway of bioactive abietane-type diterpenes with miltiradiene as the precursor (a) and sequence alignment of diterpene synthases (b). (a) *SmMDS* catalyses GGPP to (+)-CPP in class II active site and (+)-CPP to miltiradiene in class I active site. Miltiradiene is the precursor of triptolide, ecabet sodium and carnosol. (b) Sequence alignment of single product diterpene synthases *SmMDS* and *PaISO* and multiproduct diterpene synthases *PaLAS* and *AgAS*. The amino acids E690, S717 and H721 in *SmMDS* are labelled.

copalyl diphosphate synthase from *Arabidopsis thaliana* (*AtCPS*; Köksal et al., 2011) and bifunctional abietadiene synthase from *Abies grandis* (*AgAS*; Zhou et al., 2012a). Compared to abietadiene, levopimaradiene and neoabietadiene (multiple conjugated double-bond products of *AgAS*), miltiradiene contains the specific cyclohexa-1,4-diene structure of the distal ring (Gao et al., 2009). The apo-state structure of *AgAS* from gymnosperms has been determined and provides the inferred structure–function relationships underlying mixture abietadienes (Zhou et al., 2012a). The bifunctional diTPS *AgAS* produces multiple abietane-type products, but *SmMDS* strictly converts GGPP to dominant miltiradiene with characteristic double bonds (>95% of total products; Martin et al., 2004; Vogel et al., 1996). Thus, we focused on the structure–function catalytic mechanisms to produce diverse abietane backbones and the precise control over carbocation intermediates in the reaction.

Here, through sequence alignment of *SmMDS* and other class II and class I diTPSs, by site-directed mutagenesis, we identified E690 mutagenesis leads to multiproduct sandaracopimaradiene and miltiradiene. We further determined the apo-state and GGPP-bound state crystal structures of *SmMDS*, providing the possible catalytic structural mechanism of the bifunctional active pockets and the transportation of (+)-CPP. Our findings are a good example of the intermediate product transport mode in a bifunctional diTPS and the mechanisms by which *SmMDS* control the fate of carbocations to generate a single product.

Results

Sandaracopimaradiene supports the conformation of intermediate pimar-15-en-8-yl⁺

Bifunctional *SmMDS* catalyses protonation-initiated cyclization of GGPP to (+)-CPP and converts (+)-CPP to miltiradiene based on ionization-initiated cyclization (Figure 1a; Sugai et al., 2011). *SmMDS* showed high homology with *AgAS* (identity = 38.36%), isopimaradiene synthase from *Picea abies* (*PaISO*, identity = 38.67%) and the levopimaradiene/abietadiene synthase from *Picea abies* (*PaLAS*, identity = 37.84%;

Keeling et al., 2008). All of these enzymes are bifunctional class II/class I diTPSs that share the same intermediate (+)-CPP. *AgAS* and *PaLAS* convert (+)-CPP to multiple products that have the same abietane-type skeleton as miltiradiene, while *PaISO* produces the single pimarane-type product isopimaradiene. We focused on the relationship between amino acid specificity and product complexity and analysed the sequence alignment to delineate the amino acid differences in the second active site that determine product diversity. Three crucial residues, namely E690, S717 and H721, which are unique in *SmMDS* and *PaISO*, are most likely to modulate product diversity. Compared to key residues in multiproduct diTPSs, E690, S717 and H721 were special in *SmMDS*, while these positions were occupied by tyrosine, alanine and valine in *AgAS* and *PaLAS* (Figure 1b).

The enzyme activity of the E690Y mutant decreased significantly. After extending the reaction time and adding more substrates, the E690Y mutant produced no detectable products. Previous research reported that the *PaISO*:H694Y mutation resulted in a slight amount of the products sandaracopimaradiene and isopimaradiene (Keeling et al., 2008). We hypothesized that the outcome alteration was derived from the replacement of carboxyl groups with hydroxyl groups in the side chain, whereas the enzyme inactivity of *SmMDS*:E690Y may be caused by too long side chain. Then, we constructed a slightly shorter hydroxylated side chain mutant, E690S, and found that it exhibited partial enzyme activity. Moreover, E690S can also convert GGPP to a new product, sandaracopimaradiene, which was identified by comparing the mass spectra of GC–MS results with previously characterized enzyme products (Hall et al., 2013; Figures 2a and S1).

To investigate different amino acid substitution effects on E690, we further performed saturation mutagenesis experiments (Figure 2b). E690Q, which has similar side chain length with WT, had the highest enzyme activity in all of the mutants. E690 mutants that have hydrophobic side chain, namely E690I, E690L, E690V and E690M, all had lower enzyme activity, or no enzyme activity (E690A). E690T, E690C and E690N, which have similar

polar neutral side chains to E690S, produced sandaracopimaradiene and miltiradiene. Besides, E690G and E690H were also multiproduct mutants that produce sandaracopimaradiene and miltiradiene. Other too long or special side chain substitutions, that were E690W, E690R, E690F, E690K and E690P, all had no detectable products. Surprisingly, similar property but shorter side chain substitution, E690D, totally abolished its enzyme activity. These results highlighted the importance of residue E690 and also shed light on the rational enzyme design focusing on amino acid property and length.

AgAS:A723S leads to pimaradiene production, while both PaLAS:A713S and PaISO:S721A result in isopimaradiene and sandaracopimaradiene (Wilderman and Peters, 2007). The enzyme activity of *SmMDS*:S717A was almost the same as that of *SmMDS* and produce only miltiradiene, as well as that of *SmMDS*:S717G (Figure 2b). Single mutant *SmMDS*:S721V totally abolished its enzyme activity (Figure 2b). The catalytic activity of the double mutant *SmMDS*:S717A/H721V was reduced. After extending the reaction time and adding more substrates, S717A/H721V catalysed GGPP to form a series of small products with a molecular ion peak at m/z 272 (Figure S2).

The *SmMDS*:E690S and similar polar neutral side chain amino acid substitutions indicate that *SmMDS* catalysed (+)-CPP to generate the pimar-15-en-8-yl⁺ intermediate, and deprotonation of the carbocation resulted in sandaracopimaradiene (Figure 2c).

E690 determines the abietane-type transformation of miltiradiene. The single mutation effect of S717 did not seem obvious in *SmMDS*, while the double mutant S717A/H721V resulted in small alterations. These results made us consider what the choreographed reaction process is and how specific amino acids participate in and affect the reaction. Meantime, we solved the crystal structure of *SmMDS* and attempted to reveal the mechanism of tricycle diterpene formation.

Overall structure and functional analysis of *SmMDS*

First, we solved the crystal structure of *SmMDS* in its apo state (Table S1). The crystal structure contains residues 94–867 and an additional LEHHHHH tag at the C-terminus. The enzyme with the truncation of the N-terminal residues 1–93 retains catalytic activity (Figure S3) and adopts the classical $\alpha\beta\gamma$ module of plant diTPSs (Figure 3a). We superposed the *SmMDS* structure with three available plant diTPS structures, which showed RMSD values for C α of 2.1, 1.8 and 1.6 Å for monofunctional TbTS, monofunctional AtCPS and bifunctional AgAS, respectively, suggesting that they all have a similar overall architecture (Figures S4d,e,h, S5 and S6; Robert and Gouet, 2014).

To obtain the binding states of *SmMDS*, we soaked crystals of *SmMDS* and different mutants with the substrate GGPP and/or miltiradiene. Fortunately, we observed the density for GGPP in a WT structure named as *SmMDS*^{4h}, whose crystal were soaked

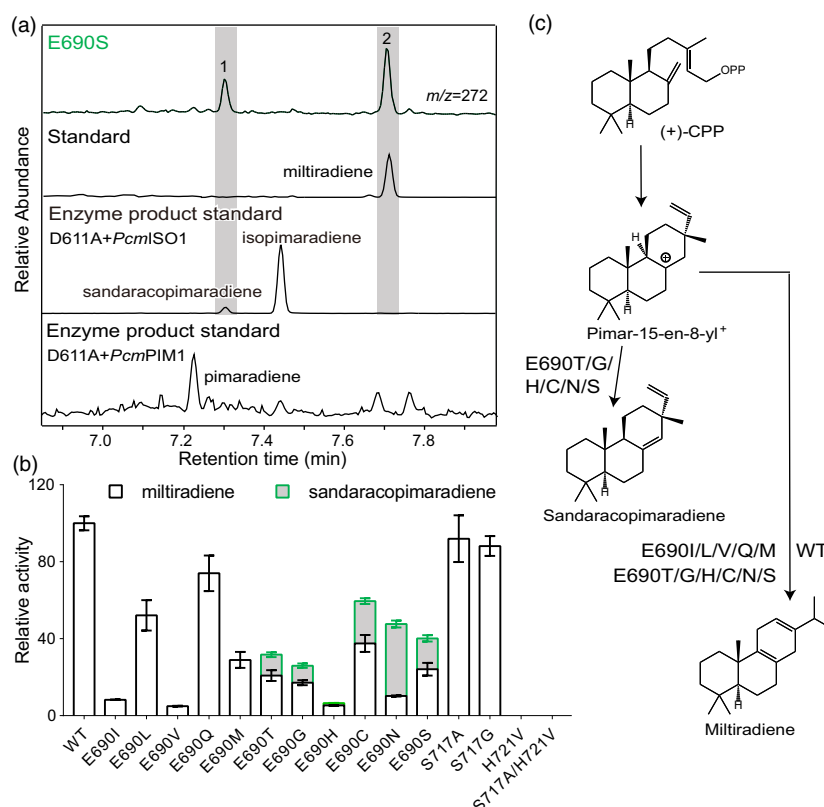


Figure 2 Effects of E690 and related residue substitutions on *SmMDS* production outcome. (a) Extracted ion chromatograms (m/z 272) from GC–MS analysis of the standard miltiradiene and products formed by E690S, D611A+PcmISO1 and D611A+PcmPIM1. The enzyme products of D611A+PcmISO1 and D611A+PcmPIM1 present authentic standards of sandaracopimaradiene, isopimaradiene and pimaradiene. (b) Relative activity of different mutants of *SmMDS*. (c) Pimar-15-en-8-yl⁺ is the proposed intermediate in the biosynthesis pathway of abietane-type diterpenes. E690T, E690G, E690H, E690C, E690N and E690S (E690T/G/H/C/N/S) catalyse (+)-CPP to sandaracopimaradiene and miltiradiene. E690I, E690L, E690V, E690Q and E690M (E690I/L/V/Q/M) catalyse (+)-CPP to miltiradiene.

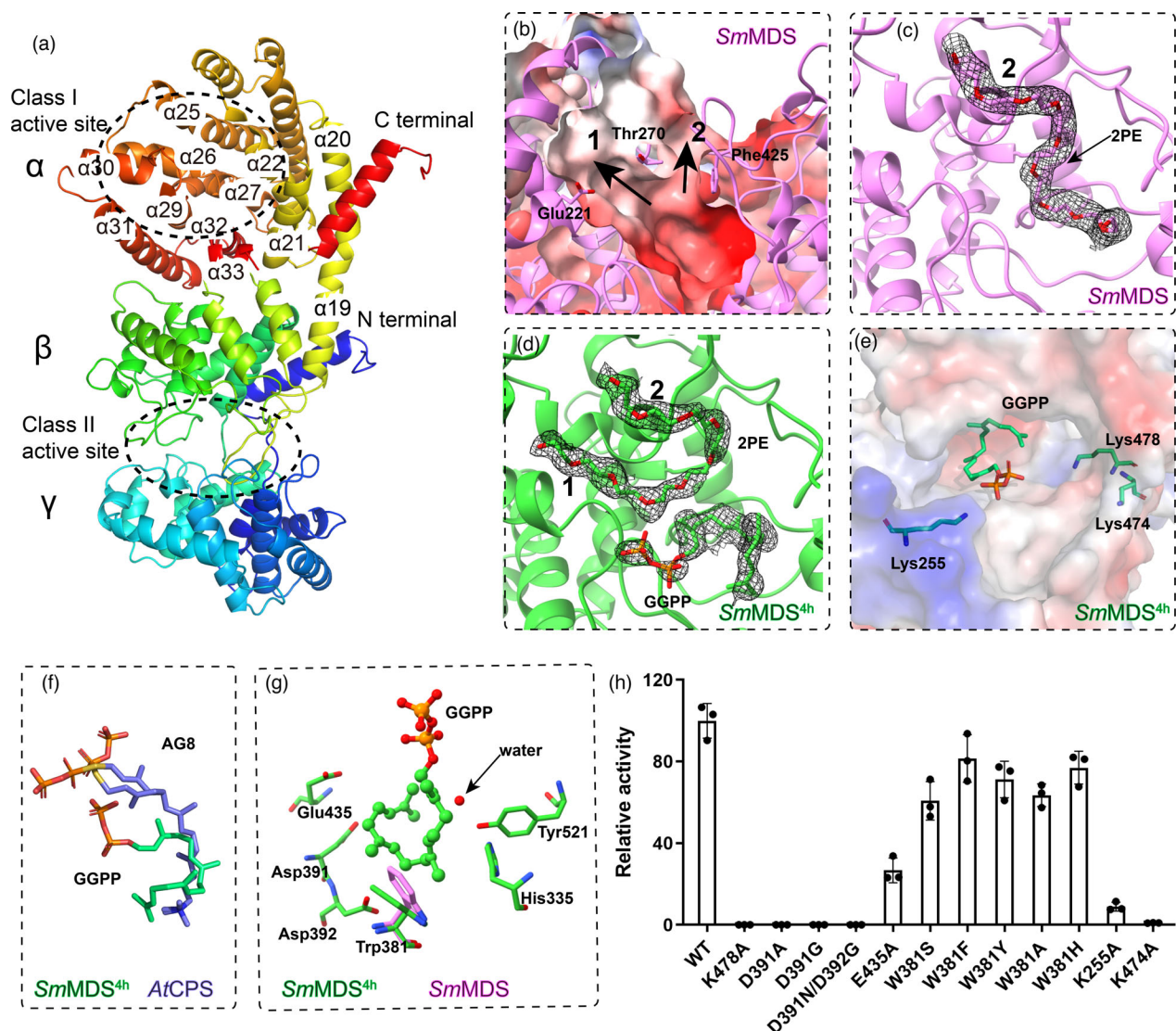


Figure 3 The overall structure of *SmMDS* and class II active site. (a) The structure of *SmMDS* is coloured in a rainbow mode. The active sites are indicated by circles. (b) Class II active site entrance is separated into two tunnels. *SmMDS* is coloured violet. (c, d) The 2Fo-Fc map of GGPP and 2PE when constructed in structure (sigma level = 0.6). *SmMDS* is coloured violet and *SmMDS*^{4h} is coloured lime green. (e) The protein surface electrostatic potential map of class II active site from *SmMDS*^{4h} structure. GGPP and key residues are shown as sticks. The red is for negative potential, white at zero, and blue is for positive. (f) Structure comparison of GGPP from *SmMDS*^{4h} (lime green) and substrate analogue AG8 from *AtCPS* (PDB ID: 3PYA, slate). (g) Key residues in the class II active site. Side chain of Trp381 in *SmMDS* is shown in violet. (h) The relative activity of key residue mutants around the class II active site. All reaction times were limited to comparing relative activities.

with GGPP for 4 h (Table S1). *SmMDS* and *SmMDS*^{4h} structures differed in the conformation of amino acids around the two active pockets, especially in the class I active pocket (Figure S4a,b). In the *SmMDS* structure, α 33 (residues 839–844) showed strong electron density, and the downstream residues 845–850 were not modelled in the structure because of weak electron density. In the *SmMDS*^{4h} structure, the density of residues 839–850 was not present. This region is predicted to adopt a loop conformation as the corresponding region in *TbTS* (Figure S4c). Deletion of residues 841–867 from *SmMDS* (*SmMDS*^{1–840}) significantly impaired *SmMDS* activity, while the *SmMDS*^{1–846} truncation retained enzyme activity (Figure S3), suggesting that residues 841–846 play an important role in maintaining enzyme activity. Based on the structures, we propose that residues 840–850 form

a flexible loop that may turn to the class I active site during the class I active site reaction.

Structure analysis of class II active site

The entrance of class II active site is separated into two tunnels by Thr270 (Figure 3b). We name the tunnel between residues Glu221 and Thr270 as tunnel 1, while the tunnel between Thr270 and Phe425 as tunnel 2. In the apo state, we observed a continuous rope-shaped density occupies part of the class II active site and the tunnel 2, which we assume to be a small molecule from the cell extract. While in the *SmMDS*^{4h} structure, the continuous rope-shaped density becomes weaker and moved from the active cavity to tunnel 1 (Figure S7). Using Ligand_identification (Terwilliger *et al.*, 2007) wizard from PHENIX, the rope-

shape density was predicted to be corresponding to a non-aethylene glycol (2PE) molecule which was constructed in many crystal structures as a exogenous molecule from *Escherichia coli*. Thus, we temporarily construct 2PE molecule, which fits the electron density well (Figure 3c,d). Besides, substrate GGPP can be modelled in the class II active site of *SmMDS*^{4h} structure perfectly, in which the pyrophosphate group has the occupancy of 0.5 (Figure 3d).

In the previously reported structure of *AtCPS* in complex with the GGPP analogue AG8 (Köksal *et al.*, 2011), the class II active site was shown to be relatively narrow than that of *SmMDS*, mainly because of that loop 457–468 in the *AtCPS* structure is in a more compact conformation than loop 468–479 in the *SmMDS* structure (Figures S4g and S5). The distinct pocket sizes of *AtCPS* and *SmMDS* may correlate with the mechanism by which GGPP is catalysed to different enantiomers of *ent*-CPP and CPP. The substrate analogue AG8 in *AtCPS* is located in a limited space, and the phosphate part has dual conformations (Figure 3f). In *SmMDS*^{4h} structure, the pyrophosphate is predicted flexible and the constructed part interacts with the density that 2PE is located (Figure 3d). Lys478 contributes to the only positive part in the class II active pocket and mutating Lys478 to alanine lost the enzyme activity totally (Figure 3e,h). So, we infer that the dynamic pyrophosphate of *SmMDS* could possibly interact with Lys478 in catalytic process.

The DXDD motif is located in the isoprene terminal part of GGPP. Mutating residues around the isoprene part of GGPP affected the enzyme activity differently (Figure 3g,h). D391A, D391G and D391N/D392G mutants abolished the entire enzyme activity. E435A mutant had partial enzyme activity. In *AgAS*, the tyrosine-histidine dyad is speculated as the catalytic base in which mutating histidine to alanine produced hydroxylated derivatives of CPP (Criswell *et al.*, 2012; Mafu *et al.*, 2015; Potter *et al.*, 2014). After soaking with GGPP, a water molecule appeared between Tyr521 and His335, other than the predicted possible catalytic base dyad (Tyr273 and His335), which indicates that Tyr521 may assist the possible catalytic base dyad in *SmMDS* catalysing process (Figure 3g).

Compared to the class II active site in the two previously solved structures, the most significant change site is Trp381 (Figure 3g). Trp381 is not strictly conserved (Figure S5). The corresponding residue in a CPS from *Salvia miltiorrhiza* is serine, and serine substitution of tryptophan reduced its catalytic activity by more than 100-fold in the production of (+)-CPP (Cui *et al.*, 2015). While in *SmMDS*, the enzyme activities of mutants W381F, W381Y, W381H, W381S and even W381A were all decreased slightly, indicating that W381 is replaceable in *SmMDS* (Figure 3h). We found that two positively charged residues, Lys255 and Lys474, are highly conserved among CPSs but exhibit considerably different conformations in the *SmMDS* structure compared to those in the *AtCPS* and *AgAS* structures (Figures 3e and S5). The two residues are located at the entrance of the class II active site, and mutating either residue affected the enzyme activity to different degrees (Figure 3e,h). On the basis of these results, we propose that in addition to the residues located in the pocket, other residues near the pocket entrance influence catalysis. Residues K255 and K474 may assist substrate entry into the class II active pocket by interacting with pyrophosphate.

Produced CPP leaves from a channel

The class II active site is located at the $\beta\gamma$ interface. Mutating residues around the pocket, such as Lys478, Asp391 and

Asp392 can influence the enzyme activity. The K478A mutant almost lost its enzyme activity entirely. In addition, by analysing *SmMDS* structure, we found a relatively continuous channel that is close to K478 (Figure 4a). The channel is composed of a narrow part and a broad part with lengths of 17 and 22 Å, respectively, with the exit at the $\alpha\beta$ interface. We predict that (+)-CPP leaves the class II active pocket through this channel. To validate the internal channel, we mutated three residues within this putative channel, namely Leu437, Lys820 and Arg824. L437 is located in the narrow part of the channel, and the mutant L437R retained low activity (Figure 4b, approximately 12% activity relative to the activity of the wild-type protein). This may be because arginine has a longer side chain than leucine, and the longer side chain is able to block the channel. For K820, which is located at the channel exit, both the K820A and K820G mutants lost part of its enzyme activity (Figure 4b). R824A completely lost the catalytic activity, which perhaps led to a completely blocked channel and almost decreased the entire catalytic ability (Figure 4b).

To further investigate whether this channel is functionally important, we compared the miltiradiene-producing activity of wild-type *SmMDS* with that of a mixture of two mutated *SmMDS* proteins, D391A and D611A. As D391A and D611A possess class I and class II activity, respectively, the D391A and D611A mutant mixture can recover the whole enzyme activity if the newly produced (+)-CPP enters the class I active site *via* free diffusion (Figure S3). Our results showed that compared to the enzyme activity of the *SmMDS*, this mutant mixture exhibited significantly reduced enzyme activity (Figure 4b). Interestingly, the R824G and D611A mutant mixture restored catalytic ability of the *SmMDS* in the same level as the D391A and D611A mutant mixture did. Thus, we infer that after (+)-CPP leaves the channel, it may move towards the class I active site *via* a surface route that is currently unclear but probably lined with positively charged residues. This observation is distinct from the previously reported bifunctional *AgAS*, where the CPP intermediate is transferred between class II and class I active sites *via* free diffusion (Peters *et al.*, 2001; Zhou *et al.*, 2012a). On the basis of these observations, we propose that the structural integration of α and $\beta\gamma$ modules endows *SmMDS* with a higher miltiradiene-producing efficiency, probably by means of forming an internal transportation route between the two active sites. Notably, in a previous study, a fusion of kaurene synthase-like (KSL) and CPS from *Salvia miltiorrhiza* significantly increased miltiradiene production in an engineered yeast strain (Zhou *et al.*, 2012b). Therefore, the detailed structural information of the channel of bifunctional *SmMDS* may provide a basis for designing and optimizing a fusion protein comprising both class I and class II diTPSs activities.

The structural mechanism of converting (+)-CPP to the single product miltiradiene

In the *SmMDS*^{4h} structure, the position of α -helices surrounding the class I active site appears to be tilted to active pocket, which may be caused by enzymatic reaction after soaking with GGPP (Figure S4a,b). In the *SmMDS*^{4h} structure, α 29, α 30 and α 31 turn to the active site, which facilitates the binding of one magnesium ion by the residues in the conserved motif of **N**⁷⁵⁸**DXXT**⁷⁶²**XXXE**⁷⁶⁶ (the bold residues). The bold residues in the conserved motif **D**⁶¹¹**DXXD**⁶¹⁵ bind another two magnesium ions, thus stabilizing the pyrophosphate group. Mutating the residues that bind magnesium ions completely abolished the enzyme activity (Figure 4c).

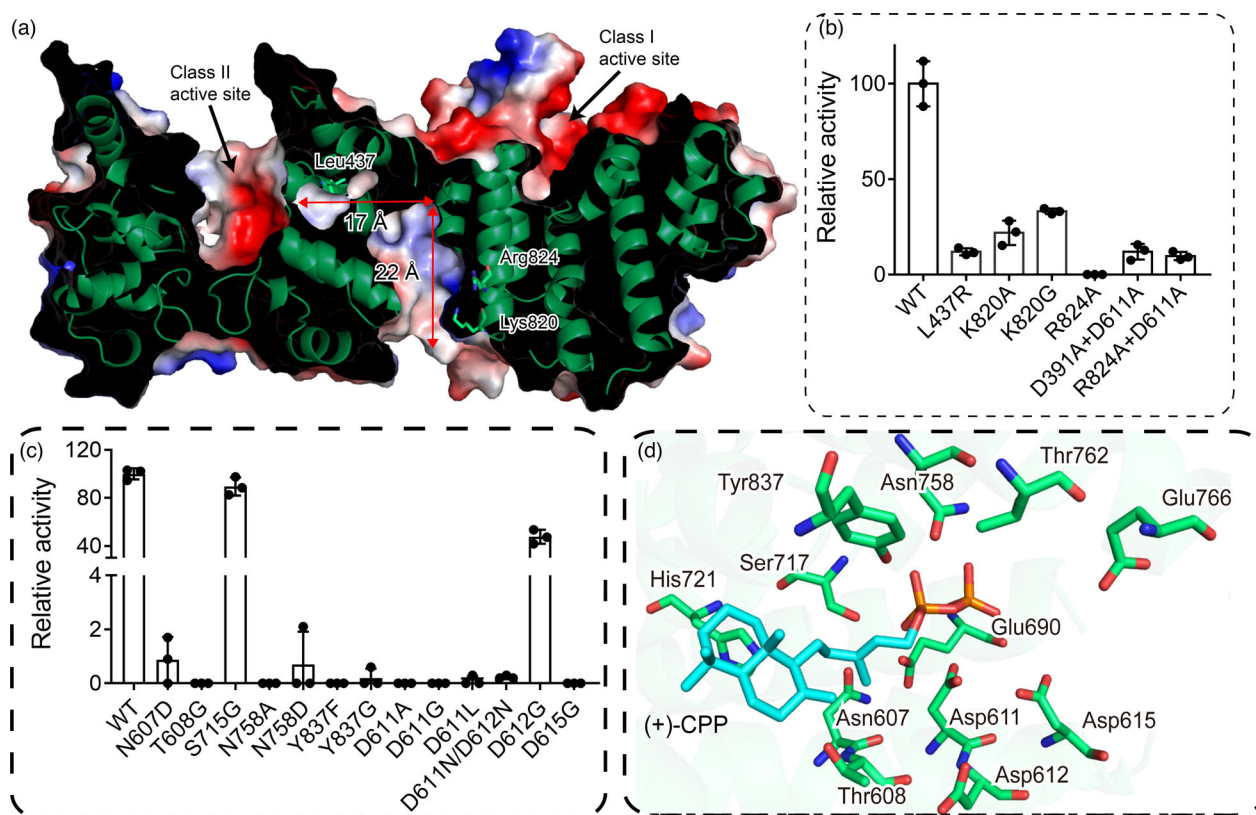


Figure 4 (+)-CPP channel and the class I active site of *SmMDS*. (a) Section view of the channel surface electrostatic potential map in *SmMDS*^{4h}. The red is for negative potential, white at zero, and blue is for positive. (b) Relative activity of mutants related to the channel. All reaction times were limited to comparing the relative activity. (c) Site-directed mutagenesis analysis of key residues involved in the cyclization of (+)-CPP to miltiradiene. All reaction times were limited to comparing the relative activity. (d) The molecular docking results of (+)-CPP (coloured cyan) to the class I active site of *SmMDS*^{4h}. Key residues related to the cyclization reaction are labelled.

The diterpene cyclization reaction can be divided into a series of carbocation intermediates that are catalysed by nearby residues or water molecules. To better understand the mechanism of the class I active site reaction, we docked (+)-CPP and miltiradiene with *SmMDS*^{4h} structure using AutoDockTools and AutoDock Vina software (Sanner, 1999; Trott and Olson, 2010; Figures 4d and S8). *SmMDS* protein were co-crystallized with miltiradiene. Interestingly, in both *SmMDS* and *SmMDS*^{4h} structures, miltiradiene-like residual density was observed in the class I active site, and its position matched to that of the docked ring structures of (+)-CPP and miltiradiene (Figure S8), thus supporting the docking results.

Around (+)-CPP, we found E690, S717, H721, and other key residues (Figures 4d and S8). Targeted mutagenesis of these residues showed that a single residue substitution can alter the product outcome. The T608G mutant exhibited a falling of enzyme activity compared to the enzyme activity of wild-type *SmMDS*. After extending the reaction time and adding more substrates, T608G produced a mixture of diterpene products, namely, miltiradiene and (+)-copalol (Figures 5a,b and S9a). As the single mutation resulted in multiple products, we hypothesized that (+)-CPP was converted to a (+)-copal-15-yl⁺ intermediate and that water-assisted deprotonation of this carbocation resulted in the product (+)-copalol (Figure 5b).

Multiple sequence alignment of Class I diTPSs that use (+)-CPP as substrate showed that Y837 is a highly conserved residue

(Figure S6). Both the Y837F and Y837G mutations decreased the enzyme activity of *SmMDS* (Figure 4c). After extending the reaction time and adding more substrates, Y837G produced no products, whereas Y837F generated a mixture of diterpene products with a molecular ion peak at *m/z* 272. The mixture of products was identified to be sandaracopimaradiene, miltiradiene and two other products (Figures 5c and S9b; namely peak4 and peak5). The yield of the compound corresponding to peak 4 was too low to prepare, so we investigated it using gas chromatography quadrupole time-of-flight (GC-Q/TOF). The results showed that its spectrum matched that of isopimara-9 (11),15-diene in the National Institute of Standards and Technology (NIST) library. The compound corresponding to peak 5 was identified to be aromatic abietatriene by comparing the mass spectra with prepared abietatriene (Figure S10). Abietatriene is assumedly derived from miltiradiene spontaneously, but Y837F catalysed GGPP to produce it in small amounts. We hypothesized that the hydroxyl group of the conserved Y837 stabilized intermediate carbocations during cyclization. When phenylalanine was substituted for Y837 (Y837F), the interacting status between the protein and carbocations was destabilized, resulting in multiple diterpene products.

The functional identification of mutants reveals that copal-15-yl⁺ and pimar-15-en-8-yl⁺ are key intermediates in the class I active site, which are quenched to (+)-copalol and sandaracopimaradiene, respectively. Based on structural and mutagenesis

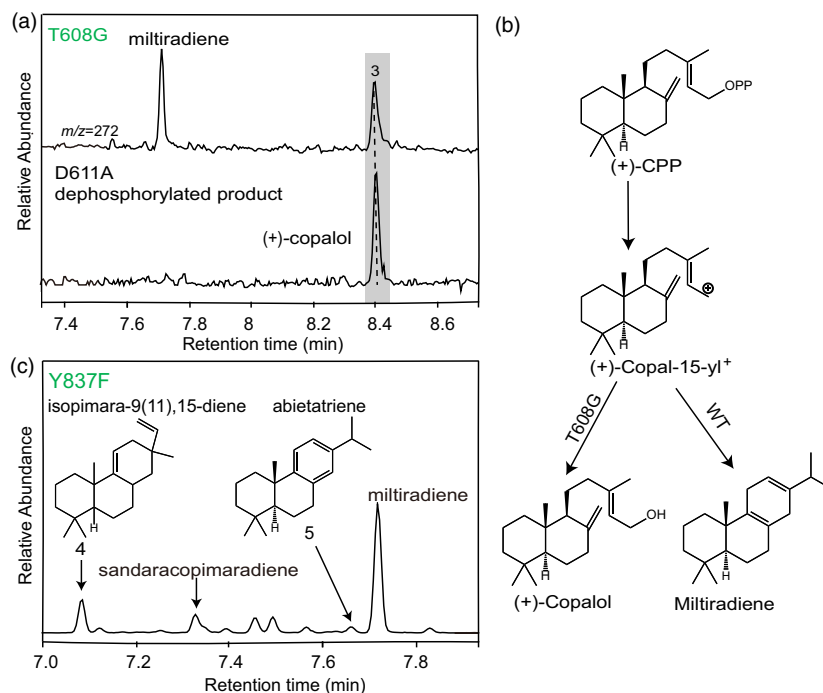


Figure 5 Effects of the T608G and Y837F mutations on the *SmMDS* product outcome. (a) GC–MS analysis of enzymatic products formed by T608G. (b) (+)-Copal-15-yl⁺ is the proposed intermediate in the biosynthesis pathway of abietane-type diterpenes. T608G catalyses (+)-CPP to (+)-copalol. (c) GC–MS analysis of enzymatic products formed by Y837F.

analyses, we proposed a structural mechanism model in which key residues stabilize intermediate carbocations during the cyclization of (+)-CPP to miltiradiene (Figure 6). The model described five intermediates (1–5) in the catalytic process. At the beginning of the catalysis reaction, the class I active site utilizes a trinuclear metal cluster triggering the ionization of the isoprenoid substrate (+)-CPP, resulting in the loss of diphosphate abstraction. The ionization of (+)-CPP leads to an allyl cation that can be drawn with two mesomeric structures, namely copal-15-yl⁺ (intermediate 1) and intermediate 2. Then, the carbocation transfers to form the pimar-15-en-8-yl⁺ (the intermediate 3). Subsequently, the specific C8–C9 double bond formed at intermediate 4, with the participation of Y837, S717, H721 and E690. Moreover, based on our molecular docking results, both E690 and Y837 are located at the newly formed ring of miltiradiene and may participate in the final 1,2-methyl migration of intermediate 4 to intermediate 5.

Discussion

Here, we successfully determined the *apo* and GGPP-bound state crystal structures of *SmMDS* and explored the precise control over copal-15-yl⁺ and pimar-15-en-8-yl⁺ intermediates in the presence of enzyme and further demonstrated an effective transport mode of (+)-CPP. As described for multiple sequential post-transition-state bifurcations, the inferred pimar-15-en-8-yl⁺ rearrangement mechanisms in the absence of enzymes have significant implications for ensuing selectivity prediction and controlling biosynthesis of complex organic reactions in general⁶. Early mechanistic work by Ravn *et al.* (2002) demonstrated the intermediacy of pimar-15-en-8-yl⁺ (intermediate 3) in the cyclization of (+)-CPP to

a mixture of abietadiene double-bond isomers catalysed by *AgAS*. From the intramolecular proton transfer perspective, later work by Wilderman and Peters (2007) suggested that a shift from intermediate 3 to isopimar-8(14)-en-15-yl⁺ was needed. However, here we demonstrate that copal-15-yl⁺ is an intermediate derived from the cleavage of the (+)-CPP diphosphate group, while pimar-15-en-8-yl⁺ (intermediate 3) is the intermediate between (+)-CPP and miltiradiene. Among them, an inferred shift from the intermediate 3 to pimar-8(9)-en-15-yl⁺ (intermediate 4) provides an intermediate for the subsequent intramolecular proton transfer. *SmMDS*:T608G produced (+)-copalol as a minor component of its product output, indicating that (+)-copalol is a potential stable intermediate. Further site-directed mutagenesis of N607 and T608 around (+)-copalol suggested that a pair of charged N607 and T608 stabilizes the formation of the copal-15-yl cation intermediate. Furthermore, *SmMDS*:E690S and similar polar neutral side chain mutants lead to two isomeric products, sandaracopimaradiene and miltiradiene. Mutagenesis of residues E690, S717, H721 and Y837 around sandaracopimaradiene explained the catalysis mechanism of the C ring stereocentre in the pimar-15-en-8-yl⁺ cation intermediate. We inferred that another pair of charged S717 and H721 assists in regulating the transition state. Compared to other diTPSs with multiple products, *SmMDS* specifically has more charged amino acids in the class I active site, which perhaps produce a single product, miltiradiene, in such an enzymatic reaction (Figures 1 and S6).

In the field of metabolic engineering, perhaps one of the most arduous is controlling metabolic flux distributions, that is, how to make a particular biosynthesis route when other metabolic routes competitively share the same precursors. The biosynthesis of miltiradiene is an example facing this situation. Miltiradiene is an

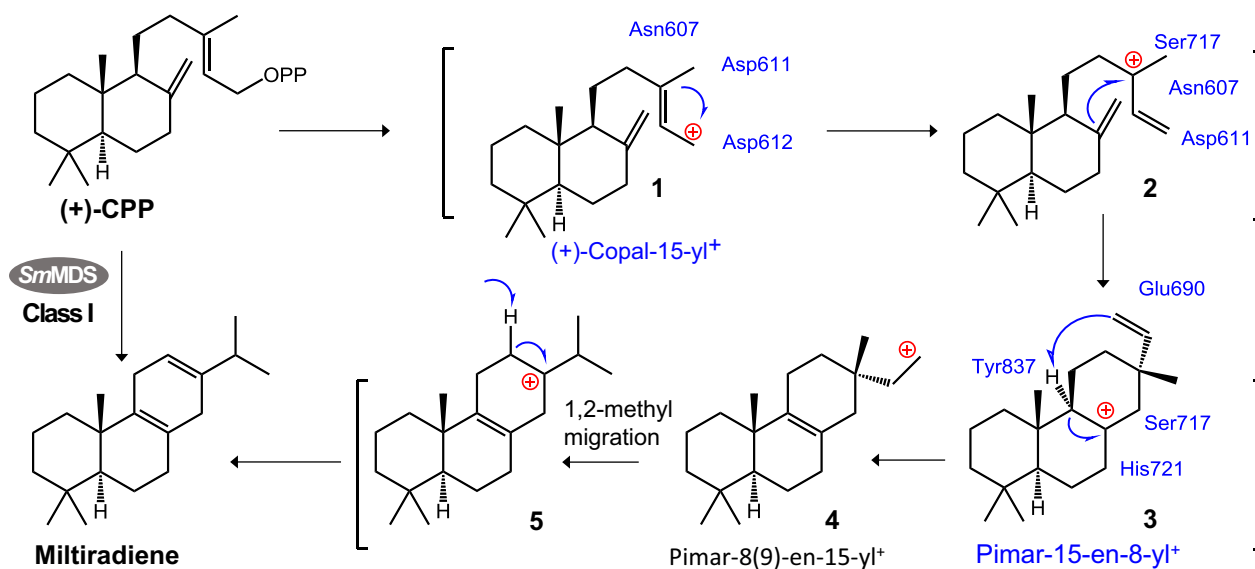


Figure 6 Cyclization mechanism of (+)-CPP to miltiradiene at the *SmMDS* class I active site. *SmMDS* catalyses (+)-CPP to miltiradiene through five intermediates, namely, intermediate **1–5**. (+)-Copal-15-yl⁺ (**1**) and pimar-15-en-8-yl⁺ (**3**) are marked blue. Curved arrows show movement of electrons. The positions of amino acid residues were drawn according to the docking results.

important precursor in the biosynthesis of tanshinones, triptolides and resin acids. Importantly, the characteristic cyclohexa-1,4-diene structure of the C ring in miltiradiene is rare in other abietane-related diterpenes. Through chimeric fusion proteins of class II and class I diTPs, more metabolic flux of (+)-CPP flowed to class I diTPs, and, as a result, the production of miltiradiene was improved, reaching a highest miltiradiene titre of 3.5 g/L in a 5-L bioreactor (Hu *et al.*, 2020). The modular architecture of chimeric fusion proteins is $\beta\alpha$ and $\gamma\beta\alpha$ (bold is the active domain); however, we directly found an inner channel in *SmMDS* with an active $\alpha\beta\gamma$ domain. This natural strategy makes (+)-CPP metabolic flux concentrated and quick, generating more miltiradiene. The production of miltiradiene and no other competitive products from (+)-CPP is undoubtedly significant to *S. moellendorffii*. The accepted hypothesis is that plant diTPs evolved from archaea by fusion of the α and $\beta\gamma$ enzymes (Moosmann and Ecker, 2020). *S. moellendorffii* belongs to an ancient lineage, namely lycophyte, which diverged shortly after land plants evolved vascular tissues (Banks *et al.*, 2011). The $\alpha\beta\gamma$ architecture of *SmMDS* may support this hypothesis from the perspective of early vascular plants.

In summary, we described the X-ray crystal structures of *SmMDS* in apo and GGPP-bound state. They are first reported structures of a bifunctional diTPs that produces only a single product. Furthermore, we proposed a catalytic mechanism taking into account the individual contributions of key active site residues. Structural and mutagenesis analyses show that copal-15-yl⁺ and pimar-15-en-8-yl⁺ are intermediates between (+)-CPP and miltiradiene. The associated molecular docking demonstrates that several key amino acid residues, such as E690, Y837, S717 and H721, precisely control intermediates and exhibit unique enzymatic selectivity. Moreover, we observed an inner channel that assisted (+)-CPP transportation, which may prevent the competition from other enzymes using (+)-CPP as a substrate in plant. Our findings advance the structural determinants of product specificity in class I active site and the transport mode of (+)-CPP in bifunctional diTPs, providing an effective strategy for the biosynthesis of high-value bioactive diterpenes.

Experimental procedures

Strains, plasmid and reagents

All the *E. coli* strains and plasmids are listed in Table S2. Phusion High-Fidelity DNA Polymerase for polymerase chain reaction (PCR) was purchased from New England Biolabs (Ipswich, MA).

Preparation of miltiradiene and abietatriene

The YJ28 strain was used to obtain the compound miltiradiene and abietatriene. Single colonies were grown in 50 mL of YPD liquid medium (1% yeast extract, 2% peptone, and 2% glucose) in a 250 mL shake flask at 30 °C and 230 rpm for 48 h (Zhou *et al.*, 2012b). The entire culture volume was transferred into 500 mL of fresh seed medium and incubated for 24 h and then transferred into 2 L of fresh seed medium and incubated for another 24 h. The seed medium was used to inoculate 8 L of fermentation medium in a New Brunswick BioFlo/CelliGen 115 bioreactor (Eppendorf, Hamburg, Germany) with a maximal working volume of 14 L. Fermentation was performed at 30 °C. During fermentation, the pH was maintained at 4.0 with the automatic addition of ammonium hydroxide, the agitation rate was kept at 250 rpm, and the dissolved oxygen was kept above 40%. Concentrated glucose solution (40%, wt/vol) was fed periodically to keep the glucose concentration above 1.0 g/L. Additional YPD medium was fed after the initial 30 h of fermentation. The culture was then harvested by extraction after 96 h of total fermentation time.

Yeast cell suspensions were concentrated at 1 L, lysed using a nano homogenizer machine (AH-1500; ATS Engineering Limited, Brampton, ON, Canada) and extracted 10 times using an equal volume of hexane. Organic fractions were pooled and dried using a nitrogen evaporator (Baojingkeji, Henan, China) and then dissolved in 10 mL of methanol before purification using preparative liquid chromatography. High-performance liquid chromatography (HPLC) separation was performed using a SHIMADZU LC-20AR (Kyoto, Japan) with a YMC HPLC column

(YMC-Pack ODS-A, 250 × 20 mmL.D., S-5 μm, 12 nm). The mobile phase, consisting of a mixture of water (A) and methanol (B), was pumped at a flow rate of 8 mL/min. The injection volume was 500 μL. The gradient elution was 100% B from 0 to 50 min.

Protein expression and purification

The coding sequence of the miltiradiene synthase gene from *S. moellendorffii* was optimized for expression in *E. coli*. The full and truncated fragments were amplified by PCR and inserted into the pET-24a plasmid using the *Xho*I and *Nde*I restriction sites. The plasmids were transformed into *E. coli* BL21-(DE3) competent cells (TransGen Biotech, Beijing, China). The bacteria were grown at 37 °C to an optimal density at 600 nm (OD_{600}) of 0.8–1.0 and cooled to 16 °C. After adding 0.2 mM isopropyl-1-thio-β-D-galactopyranoside, the induction continued by shaking for 16–20 h. Cells were harvested by centrifugation and then resuspended in lysis buffer containing 20 mM Tris-HCl (pH 8.0), 250 mM NaCl and 20 mM imidazole. Bacteria were disrupted using an automatic cryogenic crusher and separated by centrifugation. Protein supernatant was loaded to a pre-equilibrated Ni-affinity chromatography column. The SmMDS protein with a His tag at the C-terminus was washed with lysis buffer containing 50, 100 and 300 mM imidazole. Selected fractions were concentrated using an Amicon Ultra-15 concentrator (Merck KGaA, Darmstadt, Germany). The concentrated protein was applied to a Resource Q column (GE Healthcare, Chicago, Illinois, USA) with buffer A containing 20 mM Tris-HCl (pH 8.0), 10 mM NaCl, 5 mM MgCl₂, and 2 mM dithiothreitol and buffer B containing 20 mM Tris-HCl (pH 8.0), 1 M NaCl, 5 mM MgCl₂ and 2 mM dithiothreitol. Finally, the protein was purified using Superdex™200 HR 10/300 gel filtration (GE Healthcare) with buffer containing 20 mM Tris-HCl (pH 8.0), 200 mM NaCl, 5 mM MgCl₂ and 2 mM dithiothreitol. The full-length diTPS from *Pinus contorta* that catalyses (+)-CPP to isopimaradiene and sandaracopimaradiene (*PcmISO1*) and a diTPS from *P. contorta* that catalyses (+)-CPP to pimaradiene (*PcmPIM1*) with a His tag at N-terminus were purified by a Ni-affinity chromatography column.

Crystallization and data collection

The SmMDS protein was concentrated at 8 mg/mL (with 2 mM miltiradiene) for crystal screening. SmMDS crystals were grown at 16 °C by the hanging drop method using 1 μL of protein, 0.8 μL reservoir buffer and 0.2 μL of crystal seeds. The reservoir contains 0.1 M MES (pH 6.5) and 22% (v/v) poly (ethylene glycol) methyl ether (PEG 2000 MME). To obtain crystals of the SmMDS-GGPP complex, 0.2 μL of 20 mM GGPP was added to the hanging drop to a final concentration of 2 mM, and the crystals were soaked for different times. Finally, crystals were dehydrated using reservoir solution containing 10% glycerol (v/v) before flash freezing in liquid nitrogen for data collection.

X-ray diffraction data were collected on beamlines BL18U and BL19U at the Shanghai Synchrotron Radiation Facility (SSRF). SmMDS and SmMDS^{4h} diffraction data were processed with HKL2000 (Otwinowski and Minor, 1997).

Structure determination

The crystal belonged to the space group $P2_12_12_1$, and the phase was determined by the molecular replacement (MR) method using the AgAS structure (PDB ID: 3S9V). Electron density maps were calculated by PHENIX (Adams *et al.*, 2010). Model building was performed using Coot (Emsley *et al.*, 2010) and refined with PHENIX. The structures of CPP, copalol and

sandaracopimaradiene were downloaded from the PubChem website, and the .cif files were generated using PHENIX. The final structure was analysed by PHENIX. Data collection and refinement statistics are presented in Table S1.

Site-directed mutagenesis

Mutants were constructed by PCR using an overlap extension strategy with pET-24a-truncated SmMDS (90–867) as a template. Following PCR, *Dpn*I was used to digest the wild-type template. The digested product was then transformed into *E. coli* DH5α chemically competent cells. The mutants were verified by sequencing.

Enzyme activity assays

In vitro enzyme activity assays were performed in a 100 μL reaction system containing 50 μg of purified enzymes and 2.5 μg of GGPP (Sigma Aldrich, St. Louis, Missouri, USA) for 2 h at 16 °C, except for assays with the E690A, T608, S717A and Y837G mutants, which required more substrates and extended incubation times to detect products (10 μg of GGPP for 24 h). The reaction mixture was then extracted three times with a threefold volume of n-hexanes, followed by GC-MS analysis, which was carried out on a DB-5MS column (15 m × 0.25 mm × 0.10 μm film thickness) using helium as a carrier gas. The initial oven temperature was set at 50 °C for 2 min followed by a 40 °C/min gradient to 170 °C, and 20 °C/min gradient to 240 °C, 40 °C/min gradient to 300 °C and held at 300 °C for 1 min.

Mutant product identification

The product of the first active site remains as diphosphate, so calf intestinal (CIP) alkaline phosphatase (New England Biolabs) was used to hydrolyse phosphate. The dephosphorylation product copalol was also determined using GC-MS analysis. After verification of the product, miltiradiene and copalol were quantified by GC-MS analysis. Miltiradiene was extracted and prepared from the fermentation product of strain YJ28. We also obtained abietatriene, the spontaneously oxidized product of miltiradiene.

PcmISO1 (NCBI accession numbers: JQ240314), a diTPS from *P. contorta*, catalyses (+)-CPP to isopimaradiene and sandaracopimaradiene. *PcmPIM1* (NCBI accession numbers: JQ240316), a diterpene synthase from *Pinus contorta*, catalyses (+)-CPP to pimaradiene (Hall *et al.*, 2013). The sequences of *PcmISO1* and *PcmPIM1* were synthesized by Shanghai Generay Biotech Co., Ltd., Shanghai, China. Since the D611A mutant generates (+)-CPP when co-incubated with GGPP, the catalytic products of the *PcmISO1* and D611A mixture when co-incubated with GGPP are isopimaradiene and sandaracopimaradiene. Pimaradiene is the product of the *PcmPIM1* and D611A mixture with GGPP as the substrate.

Acknowledgements

We are grateful to the staffs from BL17U, BL18U and BL19U beamlines at Shanghai Synchrotron Radiation Facility for their assistance during data collection. This work is financially supported by the National Natural Science Foundation of China (82003894, 31670750, 81891010, and 81773830), National Key R&D Program of China (2020YFA0908000) and Key project at central government level: The ability to establishment of sustainable use for valuable Chinese medicine resources (2060302).

Conflict of interest

The authors declare no competing financial interest.

Author contributions

Y.T. and X.M. contributed equally to this work. Y.T., X.M., W.G., L.H. and T.J. conceived the idea. Y.T. and X.M. designed the construct; developed the purification procedure; purified the MDS protein for crystallization and functional experiments; performed crystallization trials and ligand soaking assay; performed the docking. X.M. solved the structure. Y.T. performed enzymatic activity *in vitro*, GC–MS analysis and product identification. T.H., G.C. and W.G. helped with GC–MS analysis and product identification. P.S. and K.C. prepared miltiradiene from fermentation. H.X. helped with protein purification. Y.T., X.M. and T.J. wrote the manuscript with input from all other authors.

Data availability statement

The atomic coordinates of the *Sm*MDS and *Sm*MDS^{4h} have been deposited to the Protein Data Bank with the accession number 7WAT and 7Y47, respectively. The supporting information is in Tables S1, S2 and Figure S1–S10.

References

- Adams, P.D., Afonine, P.V., Bunkóczi, G., Chen, V.B., Davis, I.W., Echols, N., Headd, J.J. *et al.* (2010) PHENIX: a comprehensive Python-based system for macromolecular structure solution. *Acta Crystallogr. D Biol. Crystallogr.* **66**, 213–221.
- Andersen-Ranberg, J., Kongstad, K.T., Nielsen, M.T., Jensen, N.B., Pateraki, I., Bach, S.S., Hamberger, B. *et al.* (2016) Expanding the landscape of diterpene structural diversity through stereochemically controlled combinatorial biosynthesis. *Angew. Chem. Int. Ed. Engl.* **55**, 2142–2146.
- Banks, J.A., Nishiyama, T., Hasebe, M., Bowman, J.L., Gribskov, M., dePamphilis, C., Albert, V.A. *et al.* (2011) The *Selaginella* genome identifies genetic changes associated with the evolution of vascular plants. *Science*, **332**, 960–963.
- Bozic, D., Papaefthimiou, D., Bruckner, K., de Vos, R.C., Tsoleridis, C.A., Katsarou, D., Papanikolaou, A. *et al.* (2015) Towards elucidating carnosic acid biosynthesis in Lamiaceae: functional characterization of the three first steps of the pathway in *Salvia fruticosa* and *Rosmarinus officinalis*. *PLoS One*, **10**, e0124106.
- Bruckner, K., Bozic, D., Manzano, D., Papaefthimiou, D., Pateraki, I., Scheler, U., Ferrer, A. *et al.* (2014) Characterization of two genes for the biosynthesis of abietane-type diterpenes in rosemary (*Rosmarinus officinalis*) glandular trichomes. *Phytochemistry*, **101**, 52–64.
- Christianson, D.W. (2017) Structural and chemical biology of terpenoid cyclases. *Chem. Rev.* **117**, 11570–11648.
- Criswell, J., Potter, K., Shephard, F., Beale, M.H. and Peters, R.J. (2012) A single residue change leads to a hydroxylated product from the class II diterpene cyclization catalyzed by abietadiene synthase. *Org. Lett.* **14**, 5828–5831.
- Cui, G., Duan, L., Jin, B., Qian, J., Xue, Z., Shen, G., Snyder, J.H. *et al.* (2015) Functional divergence of diterpene synthases in the medicinal plant *Salvia miltiorrhiza*. *Plant Physiol.* **169**, 1607–1618.
- Ding, B., Wahid, M.A., Wang, Z., Xie, C., Thakkar, A., Prabhu, S. and Wang, J. (2017) Triptolide and celastrol loaded silk fibroin nanoparticles show synergistic effect against human pancreatic cancer cells. *Nanoscale*, **9**, 11739–11753.
- Emsley, P., Lohkamp, B., Scott, W.G. and Cowtan, K. (2010) Features and development of Coot. *Acta Crystallogr. D Biol. Crystallogr.* **66**, 486–501.
- Gao, W., Hillwig, M.L., Huang, L., Cui, G., Wang, X., Kong, J., Yang, B. *et al.* (2009) A functional genomics approach to tanshinone biosynthesis provides stereochemical insights. *Org. Lett.* **11**, 5170–5173.
- Hall, D.E., Zerbe, P., Jancsik, S., Quesada, A.L., Dullat, H., Madilao, L.L., Yuen, M. *et al.* (2013) Evolution of conifer diterpene synthases: diterpene resin acid biosynthesis in lodgepole pine and jack pine involves monofunctional and bifunctional diterpene synthases. *Plant Physiol.* **161**, 600–616.
- Hanson, J.R., Nichols, T., Mukhrish, Y. and Bagley, M.C. (2019) Diterpenoids of terrestrial origin. *Nat. Prod. Rep.* **36**, 1499–1512.
- He, J., Peng, T., Peng, Y., Ai, L. and Deng, Z. (2020) Molecularly engineering triptolide with aptamers for high specificity and cytotoxicity for triple-negative breast cancer. *J. Am. Chem. Soc.* **142**, 2699–2703.
- Hong, Y.J. and Tantillo, D.J. (2014) Biosynthetic consequences of multiple sequential post-transition-state bifurcations. *Nat. Chem.* **6**, 104–111.
- Hu, T., Zhou, J., Tong, Y., Su, P., Li, X., Liu, Y., Liu, N. *et al.* (2020) Engineering chimeric diterpene synthases and isoprenoid biosynthetic pathways enables high-level production of miltiradiene in yeast. *Metab. Eng.* **60**, 87–96.
- Jin, B. and Cui, G. (2017) Functional diversification of kaurene synthase-like genes in *Isodon rubescens*. *Plant Physiol.* **174**, 943–955.
- Johnson, J.J. (2011) Carnosol: a promising anti-cancer and anti-inflammatory agent. *Cancer Lett.* **305**, 1–7.
- Keeling, C.I., Weisshaar, S., Lin, R.P. and Bohlmann, J. (2008) Functional plasticity of paralogous diterpene synthases involved in conifer defense. *Proc. Natl. Acad. Sci. USA*, **105**, 1085–1090.
- Köksal, M., Hu, H., Coates, R.M., Peters, R.J. and Christianson, D.W. (2011) Structure and mechanism of the diterpene cyclase ent-copalyl diphosphate synthase. *Nat. Chem. Biol.* **7**, 431–433.
- Köksal, M., Jin, Y., Coates, R.M., Croteau, R. and Christianson, D.W. (2011) Taxadiene synthase structure and evolution of modular architecture in terpene biosynthesis. *Nature*, **469**, 116–120.
- Liu, X., Zhao, P., Wang, X., Wang, L., Zhu, Y. and Gao, W. (2019) Triptolide induces glioma cell autophagy and apoptosis via upregulating the ROS/JNK and downregulating the Akt/mTOR signaling pathways. *Front. Oncol.* **9**, 387.
- Mafu, S., Potter, K.C., Hillwig, M.L., Schulte, S., Criswell, J. and Peters, R.J. (2015) Efficient heterocyclisation by (di)terpene synthases. *Chem. Commun.* **51**, 13485–13487.
- Martin, D.M., Faldt, J. and Bohlmann, J. (2004) Functional characterization of nine Norway Spruce TPS genes and evolution of gymnosperm terpene synthases of the TPS-d subfamily. *Plant Physiol.* **135**, 1908–1927.
- Moosmann, P. and Ecker, F. (2020) A monodomain class II terpene cyclase assembles complex isoprenoid scaffolds. *Nat. Chem.* **12**, 968–972.
- Otwinowski, Z. and Minor, W. (1997) Processing of X-ray diffraction data collected in oscillation mode. *Methods Enzymol.* **276**, 307–326.
- Pateraki, I., Andersen-Ranberg, J., Hamberger, B., Heskes, A.M., Martens, H.J., Zerbe, P., Bach, S.S. *et al.* (2014) Manoyl oxide (13R), the biosynthetic precursor of forskolin, is synthesized in specialized root cork cells in *Coleus forskohlii*. *Plant Physiol.* **164**, 1222–1236.
- Peters, R.J., Ravn, M.M., Coates, R.M. and Croteau, R.B. (2001) Bifunctional abietadiene synthase: free diffusive transfer of the (+)-copalyl diphosphate intermediate between two distinct active sites. *J. Am. Chem. Soc.* **123**, 8974–8978.
- Potter, K., Criswell, J., Zi, J., Stubbs, A. and Peters, R.J. (2014) Novel product chemistry from mechanistic analysis of ent-copalyl diphosphate synthases from plant hormone biosynthesis. *Angew. Chem. Int. Ed. Engl.* **53**, 7198–7202.
- Ravn, M.M., Peters, R.J., Coates, R.M. and Croteau, R. (2002) Mechanism of abietadiene synthase catalysis: stereochemistry and stabilization of the cryptic pimarenyl carbocation intermediates. *J. Am. Chem. Soc.* **124**, 6998–7006.
- Robert, X. and Gouet, P. (2014) Deciphering key features in protein structures with the new ENDscript server. *Nucleic Acids Res.* **42**, W320–W324.
- Sanner, M.F. (1999) Python: a programming language for software integration and development. *J. Mol. Graph. Model.* **17**, 57–61.
- Shi, W., Xu, G., Zhan, X., Gao, Y., Wang, Z., Fu, S., Qin, N. *et al.* (2020) Carnosol inhibits inflammasome activation by directly targeting HSP90 to treat inflammasome-mediated diseases. *Cell Death Dis.* **11**, 252.
- Su, P., Guan, H., Zhao, Y., Tong, Y., Xu, M., Zhang, Y., Hu, T. *et al.* (2018) Identification and functional characterization of diterpene synthases for triptolide biosynthesis from *Tripterygium wilfordii*. *Plant J.* **93**, 50–65.

- Sugai, Y., Ueno, Y., Hayashi, K., Oogami, S., Toyomasu, T., Matsumoto, S., Natsume, M. *et al.* (2011) Enzymatic (¹³C) labeling and multidimensional NMR analysis of miltiradiene synthesized by bifunctional diterpene cyclase in *Selaginella moellendorffii*. *J. Biol. Chem.* **286**, 42840–42847.
- Terwilliger, T.C., Adams, P.D., Moriarty, N.W. and Cohn, J.D. (2007) Ligand identification using electron-density map correlations. *Acta Crystallogr. D Biol. Crystallogr.* **63**, 101–107.
- Trott, O. and Olson, A.J. (2010) AutoDock Vina: improving the speed and accuracy of docking with a new scoring function, efficient optimization, and multithreading. *J. Comput. Chem.* **31**, 455–461.
- Vogel, B.S., Wildung, M.R., Vogel, G. and Croteau, R. (1996) Abietadiene synthase from grand fir (*Abies grandis*). cDNA isolation, characterization, and bacterial expression of a bifunctional diterpene cyclase involved in resin acid biosynthesis. *J. Biol. Chem.* **271**, 23262–23268.
- Wilderman, P.R. and Peters, R.J. (2007) A single residue switch converts abietadiene synthase into a pimaradiene specific cyclase. *J. Am. Chem. Soc.* **129**, 15736–15737.
- Zerbe, P., Chiang, A., Dullat, H., O'Neil-Johnson, M., Starks, C., Hamberger, B. and Bohlmann, J. (2014) Diterpene synthases of the biosynthetic system of medicinally active diterpenoids in *Marrubium vulgare*. *Plant J.* **79**, 914–927.
- Zhou, K., Gao, Y., Hoy, J.A., Mann, F.M., Honzatko, R.B. and Peters, R.J. (2012a) Insights into diterpene cyclization from structure of bifunctional abietadiene synthase from *Abies grandis*. *J. Biol. Chem.* **287**, 6840–6850.
- Zhou, Y.J., Gao, W., Rong, Q., Jin, G., Chu, H., Liu, W., Yang, W. *et al.* (2012b) Modular pathway engineering of diterpenoid synthases and the mevalonic acid pathway for miltiradiene production. *J. Am. Chem. Soc.* **134**, 3234–3241.

Supporting information

Additional supporting information may be found online in the Supporting Information section at the end of the article.

Figure S1 Mass spectra of sandaracopimaradiene, miltiradiene and products (peak 1 and peak 2) produced by E690S.

Figure S2 Effect of the S717A/H721V mutation on the SmMDS product outcome.

Figure S3 Functional testing of truncation variants and mutants of miltiradiene synthase.

Figure S4 Comparison of SmMDS with other structures.

Figure S5 Sequence comparison of SmMDS with other diTPSs that have an active class II active site.

Figure S6 Sequence comparison of SmMDS with other diTPSs that catalyse CPP in the class I active site.

Figure S7 The mFo-DFc map of the class II active site and the nearby tunnels.

Figure S8 The polder map in the inner part of class I active site of SmMDS4h (a, c, d) and SmMDS (b) structures.

Figure S9 Mass spectra of (+)-copalol and products produced by T608G (peak 3) and Y837F (peak 4 and peak 5).

Figure S10 Identification of the compound corresponding to peak 5 in Y837F mutation product outcome.

Table S1 Data collection and refinement statistics.

Table S2 Strains and plasmids used in this study.